

Molecular Dynamics and Free Energy Study of the Conformational Equilibria in the UUUU RNA Hairpin

Nan-Jie Deng*

Accelrys Inc., 10188 Telesis Court, San Diego, California 92121

Piotr Cieplak

Burnham Institute for Medical Research, La Jolla, California 92037

Received November 17, 2006

Abstract: A series of molecular dynamics (MD) simulations was performed to elucidate the thermodynamic basis for the relative stabilities of hairpin, duplex, and single stranded forms of the 5'-CGC(UUUU)GCG-3' oligonucleotide. According to a recent NMR study this sequence exhibits dynamic conformational equilibrium in aqueous solution in the vicinity of room temperature. Free energy calculations using the molecular mechanics-Poisson Boltzmann-surface area (MM-PB/SA) approach support a shift in the conformational equilibrium from duplex to hairpin as the temperature is increased from 276 to 300 K, in agreement with the NMR results. The effect of added salt on the relative stabilities of RNA conformers is also reproduced by our calculations. The calculated ΔH° for the equilibrium between hairpin and single stranded forms is estimated to be -23.4 kcal/mol, in reasonable agreement with experimental values. Our results reveal that the conformational equilibrium strongly depends on the solute entropy and the electrostatic interactions modulated by added salt. Simulations of hairpin loop conducted at two different temperatures converged to the same lowest energy loop conformation. This conformer is stabilized by favorable van der Waals interactions as a result of U5-U6-U7 base stacking, a hydrogen bond between the U4 base and the phosphate linking U6 and U7, and hydrogen bonds involving the 2'OH groups at U4 and U6. However, the sugar pucker of the four uridines in the lowest energy conformer is different from that reported by a NMR study. While the NMR study found that U5 and U7 adopt the C2'-endo conformation, the simulation results suggests that overall the structure with the U5 and U7 in the C3'-endo conformation is thermodynamically more stable than the structure containing the C2'-endo pucker by approximately 8 kcal/mol. Calculations based on the MM-PB/SA scheme show that although the electrostatic solvation free energy favors the C2'-endo conformation for the U5 and U7 riboses, it is offset by the less favorable intramolecular electrostatic and van der Waals energies. To enhance the conformational sampling, a replica exchange molecular dynamics (REMD) simulation was conducted in a generalized Born (GB) continuum solvent for the hairpin loop. This simulation indicates that the stable loop structure observed in the explicit solvent simulations corresponds to the free energy minimum. It also reveals that while the U4, U5, and U6 sugar rings are predominantly in the C3'-endo conformation, there is considerable variation in the sugar pucker of the U7 ribose ring.

1. Introduction

Hairpin loops are common secondary structural elements in RNA structure. RNA tetraloops contain four nucleotides

forming a loop closed by a Watson–Crick base-paired doubly helical stem. They are widely believed to play an important role in RNA folding and structure.¹ Tetraloops can also participate in RNA tertiary interactions and protein–RNA binding, serving as important molecular recognition sites.

* Corresponding author e-mail: ndeng@accelrys.com.

For example, binding of bacteria signal recognition particle (SRP) to its receptors is influenced by the structure and conformational flexibility of the tetraloop region of the 4.5S RNA.²

The UUUU tetraloop motif is found in the domain IV hairpin loops of yeast *Saccharomyces cerevisiae* SRP RNA.³ Compared with other RNA tetraloops such as the UNCG or GNRA tetraloops which are more frequently occurring and exhibit remarkable stability,⁴ the solution structure of UUUU tetraloops is more dynamic. The structural flexibility of UUUU tetraloop is believed to be important in enhancing the catalytic activity of the hammerhead ribozyme: for example, changing the loop II sequence from UUUU to the thermodynamically more stable GCAA tetraloop reduces the catalytic cleavage rate considerably for the hammerhead ribozyme variants at low Mg^{2+} concentrations.⁵

The melting temperature (T_m) and the thermodynamic parameters of a 12 nucleotide cUUUUG tetraloop have been determined in thermal denaturation experiments.^{6,7} In one study, Tinoco et al.⁶ measured the UV absorbance melting profiles at 260 nm and estimated the T_m to be 60.4 °C. More recently, Proctor et al.⁷ found $T_m = 59.2$ °C, based on measurements of both UV absorbance (at 260 and 280 nm) and NMR spectroscopy. Estimated errors in T_m are ± 1 °C in these studies. A recent NMR study on a 10 nucleotide cgcUUUUGcg tetraloop revealed interesting conformational equilibria involving duplex form, hairpin loop, and single stranded RNA.⁸ Information on the relative population of secondary structural species is obtained by measuring the temperature dependence of the 1D 1H NMR spectra. The results indicate that the duplex form is only stable at 3 °C, while the hairpin loop is a predominant species at 27 °C. At higher temperatures the hairpin melts and forms single stranded RNA. The duplex conformation is found to be favored by the addition of salt. The NMR spectroscopy also provides detailed information on the conformations of the ribose moiety in the loop composed of uridines.⁸ The pseudorotation phases and amplitudes of the ribose in the four uridines were obtained by measuring the homonuclear $^3J(H,H)$ coupling constants. The results of sugar puckering modes were corroborated by independent measurements of the heteronuclear $^nJ(C,H)$ coupling from cross-correlated relaxation experiment. According to these solution NMR studies, nucleotide U5 and U7 in the loop region are in the C2'-endo conformation, instead of the C3'-endo conformation that is consistent with the canonical A-form of RNA.

These experimental works provide motivation for the present computational investigation in which we conduct force-field based simulations on a cgcUUUUGcg tetraloop sequence. The goal of the present study is to interpret and understand the conformational properties and the energetics of the short RNA oligonucleotides and to elucidate the origins of the relative stabilities of various secondary structural forms. This is essential for a physical interpretation of the temperature dependent conformational equilibria and may be helpful in understanding the activity of the hairpin loop under different physical conditions.

Molecular dynamics (MD) simulations have been a powerful tool in studying the physical properties of nucleic

acids^{9–11} because of their ability to provide detailed structural and energetic information¹² and to reveal the time dependent conformational transitions. In recent years, a number of MD simulations studies of RNA hairpins have been carried out in explicit solvent and/or by using implicit solvent models.^{13–21} Using MD simulations in explicit solvent and MM-PB/SA approach for postanalysis, Srinivasan et al.¹³ were able to correctly discriminate between different hairpin conformations of a UUCG tetraloop. Hall and Williams^{14,21} conducted MD simulations on a UUCG tetraloop using a GB/SA implicit solvent model. In one of their studies,¹⁴ the simulated RNA hairpin showed some tendency of converting to experimental loop conformation from incorrect structures in nanosecond time scale. In another study,²¹ they examined the effect of substitution of a G-C for a C-G closing base-pair in the UUCG tetraloop by experimental and computational methods. The GB/SA simulation results are consistent with the increased chain flexibility in the UUCG tetraloop closed by the G-C base-pair. Li et al.²⁰ studied the thermal denaturation and refolding of a GAAG tetraloop by running MD simulations in both explicit solvent and a GB/SA solvent. The melting temperature obtained from the simulation is in fair agreement with experiments. Based on the structures sampled during relatively short heating and cooling cycles, they concluded that the folding of the tetraloop proceeds in a stepwise manner. Pande and coworkers^{15,17,18} have conducted a series of large scale MD simulations to investigate the folding dynamics in a GCAA tetraloop. Experimentally, the folding of this hairpin follows two-state kinetics. In their first paper on this hairpin sequence,¹⁵ folding pathways were inferred from the conformations populated along unfolding trajectories generated by multiple high-temperature MD simulations in a GB/SA solvent. The folding/unfolding was shown to be a three-state event, with a globular intermediate state separating the folded and unfolded states in the free energy surface. In the second study,¹⁸ massively parallel simulations were achieved using distributed computing network, which resulted in much more extensive sampling (hundreds of microseconds) of the configuration space. Two types of folding/unfolding pathways, compaction and zipping, are identified. Both pathways are described by two-state free energy surfaces. The importance of explicitly including the solvent and ions is underscored by their most recent simulation study using explicit solvent,¹⁷ in which the picture of two distinct folding pathways was shown to be an oversimplification. Using explicit solvent simulations, significantly greater diversity in the intermediate structures was sampled during the folding process. The folding in explicit ionic solvent was shown to be driven by the collapse of the extended structures, and no simple pathway can be easily distinguished in a highly stochastic conformational search process. Case studies of RNA hairpin simulations include a recent work by Spackova and Sponer¹⁹ on the sarcin-ricin domain motif from 23S (*Escherichia coli*) and 28S(rat) rRNA, which features a GAGA tetraloop region. This tetraloop was found to be the most dynamic part of the RNA motif, and long-residency water molecules were shown to be important in mediating non-Watson–Crick base pairing in the tetraloop.

While these studies demonstrated the usefulness of MD simulation in providing valuable insights into the conformational dynamics of the RNA hairpins at atomic resolutions, limitations in the current generation force field and the use of implicit solvent model can lead to errors in the description of conformational energy surface for noncanonical nucleic acid structures such as single stranded loops. Recently, Fadrna and co-workers²² conducted an extensive study on the four-thymidine DNA loops in guanine quadruplexes (G-DNA) using explicit solvent simulation, locally enhanced sampling (LES), and MM-PB/SA free energy calculations. They found that while the force field yields correct characterization of the G-DNA stem structure, it has problems in the description of the flexible loop region interacting with monovalent cations.

The molecular mechanics-Poisson Boltzmann-surface area (MM-PB/SA) method is an approximate approach to the calculation of the free energy difference between two conformational states. This method was first developed to estimate the relative stability of A- and B-form DNA and RNA duplex,²³ the RNA hairpin loops and helices,¹³ and the conformational preferences of A- and B-form DNA in aqueous and mixed solutions.²⁴ It considers the two end points in a configuration space, where the free energy of a structure is decomposed into contributions from the gas-phase molecular mechanics energy, the electrostatic and nonpolar components of the solvation free energy, and the solute entropy. The electrostatic component of the solvation free energy is calculated by solving Poisson–Boltzmann equation (PB) or by using the generalized Born approximation (GB) for a solute in a dielectric medium mimicking water. According to this approach the nonpolar term which accounts for the hydrophobic effect is approximated by a solvent accessible surface area (SA) term. The solute conformational entropy associated with vibrational motions in a single energy well may be obtained by normal-mode calculations. The loss of translational and rotational entropies from molecular association or binding may be estimated using expressions for ideal gas systems or by considering the change in the volume of the conformational space upon association. An ensemble of conformation is collected from snapshots along trajectories generated by running molecular dynamics simulations in explicit or implicit solvents. The MM-PB/SA approach²⁵ and its variants have been widely used to study the problems involving protein–ligand,²⁶ protein–protein,^{27,28} protein–DNA,²⁹ DNA–ligand,³⁰ and RNA–ligand binding.³¹ It has also been applied to analyze the free energies of various conformational species sampled in the 1- μ s folding simulation of villin headpiece³² and the relative stabilities of the Hoogsteen duplex, the reverse Watson–Crick parallel duplex, and the antiparallel Watson–Crick duplex of d(A:T)-based DNA molecules.³³

While the MM-PB/SA analysis can be an effective method in many situations, the simplified treatment of the solvation effects could lead to errors in estimating free energy: (1) The van der Waals interactions between the solute and solvent may be inadequately represented by the surface area SA term, which uses a single surface tension constant for all types of atoms. (2) In the continuum dielectric model

such as PB, the solvent and solute phases are considered as uniform dielectric media, which responds linearly to external electric field. It also assumes that the solvent equilibration around a given solute conformation is complete at every instant. These assumptions may be inadequate for characterizing the atomic nature of the solvent–solute interactions. For example, hydration patterns emerged from explicit solvent simulations indicate that water densities in the vicinity of the nucleic acids structures are far from uniform.^{11,34} The nonuniform distribution of water density should have an impact on the dielectric properties of the solvent phase, and such an effect is not taken into account by the current continuum electrostatics models. (3) The calculation of PB is sensitive to the choice of parameters such as the input atomic radii, the effective dielectric constant of the solute phase, and the definition of dielectric boundary separating the solute and solvent. Since the extent of errors caused by these factors is case dependent, caution is needed when applying the method and interpreting the free energy results.

In the present work, we perform a series of molecular dynamics (MD) simulations on the RNA sequence 5'-CGC-(UUUU)GCG-3' in aqueous solutions initiated from duplex, hairpin loop, and single stranded forms at 276 and 300 K. The MM-PB/SA method is applied to estimate the free energy differences among different conformational species, and the results are compared with experimental data. We investigate the energy profiles of the sugar puckering of the loop uridines and discuss the results in relation to the findings from a NMR study. The structural transition revealed from a 100 ns folding simulation in explicit solvent initiated from single stranded RNA is also analyzed. To improve the efficiency of conformational sampling, we apply replica exchange molecular dynamics (REMD) simulations in a generalized Born continuum solvent described by the GBSW model.^{35,36} We analyze the free energy surface of the hairpin and compare the results with those obtained from the explicit solvent simulations.

2. Methods

Explicit Solvent MD Simulation. The initial structures for the duplex simulations and single stranded RNA simulations were built according to the structural parameters for the standard A-form RNA. One of the initial structures used for the hairpin simulations was built using the coordinates of the cGUAAG tetraloop region in the RNA hammerhead ribozyme³⁷ (PDB ID 1mme) as a template. The four uridines in this initial structure have the C3'-endo sugar pucker, which are different from the sugar puckering modes reported from a NMR study.⁸ One aspect of the present study is to observe reversible conversions in the sugar pucker of the loop residues. To investigate the energy basis for the sugar pucker preferences, a second initial coordinate set was used in which the sugar puckering configuration was modified to resemble those determined by the NMR study, i.e., the U5/U7 are in the C2'-endo and the U4/U6 are in the C3'-endo conformation, respectively. The conformations of the three secondary structural forms are shown in Figure 1(a). The base-pairing and stacking interactions in the hairpin conformation are illustrated in Figure 1(b).

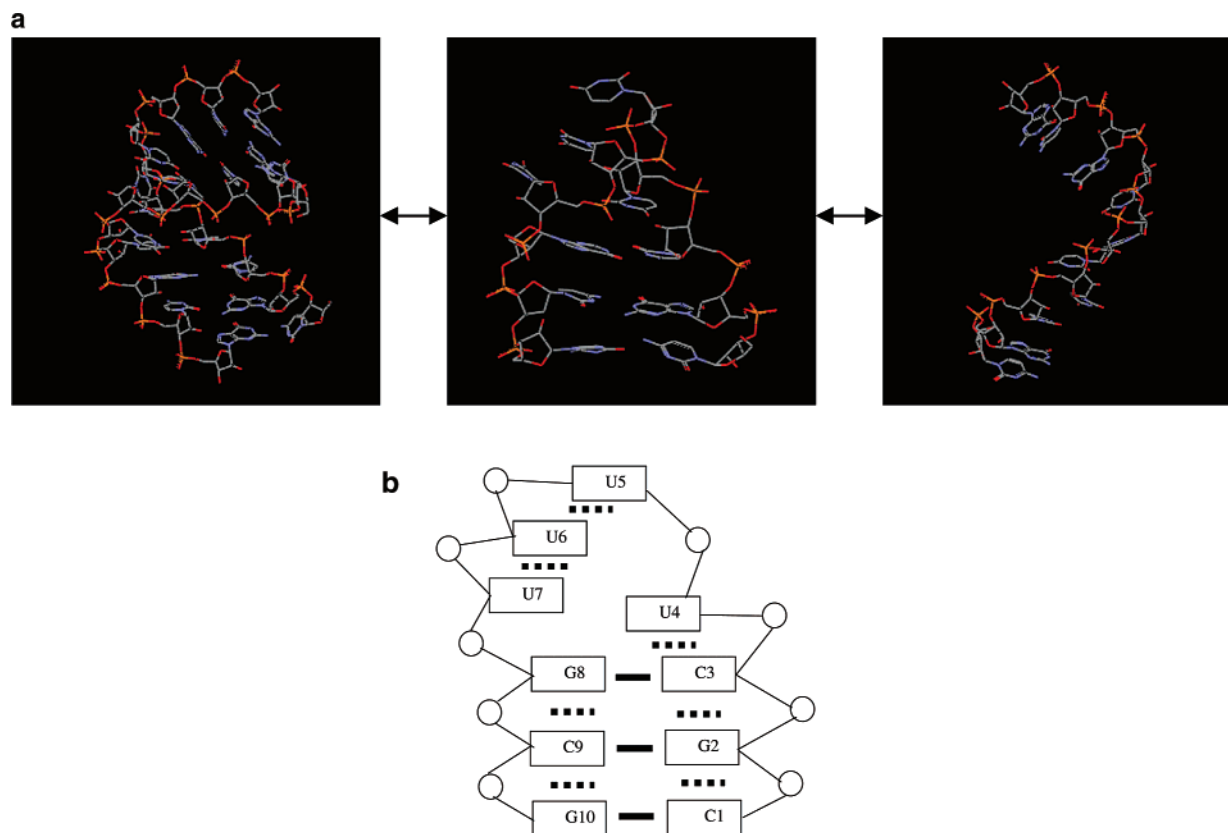


Figure 1. (a) 3D views of the three secondary structural forms. (b) Schematic diagram of the hairpin conformation: circle, phosphate group; solid line, Watson–Crick base pairing; and dotted line, base stacking interaction.

In explicit solvent simulations, sodium counterions were added to neutralize the net charges at each phosphate group. The solute molecule plus counterions were then solvated in a truncated octahedral box containing TIP3P water molecules³⁸ previously equilibrated at 300 K and 1 atm pressure, with the solute atoms separated from nearest walls of the box by 9 Å. Waters within 2.8 Å of solute atoms or counterions were removed from the solvated systems. The MD simulations were performed using the CHARMM³⁹ program versions 29b1 and 30b1. The all-atom CHARMM27 parameter set^{40,41} was used to model nucleic acid molecules. Electrostatic interactions were computed using the particle-mesh Ewald (PME) method.⁴² A switching function between 8.5 Å and 10 Å was used to calculate van der Waals interactions. The Verlet leapfrog integrator was used to solve the equation of motion with an integration step of 2 fs. MD simulations were performed in the NpT ensemble, under atmospheric pressure, using constant pressure/temperature (CPT) dynamics. In each case the following protocol has been applied to minimize and equilibrate the simulated system. Prior to the MD production run, the molecular system was equilibrated according to the following protocol: the solvent alone was first minimized for 1000 steps using the steepest descent method followed by 1000 steps of the adopted basis Newton–Raphson (ABNR) method, with the solute molecules fixed in space. The whole system was then minimized for 1000 steepest descent steps and 1000 ABNR steps without constraints. Following the minimization steps, the system was heated to the desired temperature from 50 K within 40 ps. The system was then equilibrated at the targeted

temperature for 40 ps, before the production run was started. The MD trajectories were saved every 1 ps for analysis.

Free Energy Estimations from MM-PB/SA. As described in the Introduction, a fundamental assumption in the MM-PB/SA approach is that the free energy of a structure may be decomposed into additive contributions: gas-phase molecular mechanics energy $E(\text{gas})$, solvation free energy $G(\text{solv})$, and entropic terms originating from translational, rotational, and vibrational motions of the solute molecules. The free energy of an ensemble of solute structures is obtained by taking the averages over each snapshot in the ensemble generated by molecular dynamics method, i.e.

$$\langle G(\text{tot}) \rangle = \langle E(\text{gas}) \rangle + \langle G(\text{solv}) \rangle - T \langle S(\text{tot}) \rangle \quad (1)$$

The gas-phase energy of the solute is the sum of the internal energy $E(\text{intra})$, electrostatic energy $E(\text{elec})$, and van der Waals energy $E(\text{vdw})$

$$E(\text{gas}) = E(\text{intra}) + E(\text{elec}) + E(\text{vdw}) \quad (2)$$

where the internal $E(\text{intra})$ includes energies from bond, angle, dihedral, and improper dihedral terms. The solvation free energy is further decomposed into electrostatic and nonpolar contributions and is written as

$$G(\text{solv}) = G(\text{PB}) + G(\text{np}) \quad (3)$$

The electrostatic contribution to the solvation free energy $G(\text{PB})$ accounts for the electrostatic interaction between the solute and the polarizable solvent. The latter is treated as a continuum dielectric medium, described by the Poisson–

Boltzmann equation. The nonpolar term $G(\text{np})$ includes the unfavorable hydrophobic contribution and the favorable van der Waals interaction between the solute and the solvent. This term is often assumed to be proportional to the solvent accessible surface area (SASA), i.e.

$$G(\text{np}) = \gamma \times \text{SASA} + \beta \quad (4)$$

The surface tension coefficient γ of 0.5 cal/mol·Å² and zero for constant β are used in the present study. The atomic radii set for nucleic acids derived by Banavali and Roux⁴³ for the CHARMM27 force-field parameters was used to define dielectric boundary separating solute and solvent. The Poisson–Boltzmann equation was solved by the PBEQ module in the CHARMM program, using a grid spacing of 0.4 Å and the re-entrant molecular surface for dielectric boundary.

The entropic term $T\langle S(\text{tot}) \rangle$ includes contributions from solute translation, rotation, and vibrational movements:

$$T\langle S(\text{tot}) \rangle = T\langle S(\text{trans}) \rangle + T\langle S(\text{rot}) \rangle + T\langle S(\text{vib}) \rangle \quad (5)$$

The $T\langle S(\text{trans}) \rangle$ and $T\langle S(\text{rot}) \rangle$ are calculated using the standard statistical mechanics expressions for entropies associated with rigid-body translation and rotation in ideal gas.⁴⁴

Two methods, the normal-mode analysis and the quasi-harmonic analysis (QH), are used to estimate the solute vibrational entropy. In the normal-mode analysis, we calculate the normal-mode frequencies and use the standard statistical mechanics expression for independent harmonic oscillators⁴⁴ (eq 6) to estimate the entropy due to molecular vibration:

$$TS(\text{vib}) = \sum_{i=1}^{3N-6} \left[\frac{h\nu_i}{\exp(h\nu_i/kT) - 1} - kT \ln(1 - \exp(-h\nu_i/kT)) \right] \quad (6)$$

Here ν_i is the frequency of the i th normal mode, k is the Boltzmann constant, and h is Planck's constant. Prior to normal-mode calculations, the molecular system was fully minimized using a distance dependent dielectric medium with $\epsilon = 4r$, until the root-mean-square energy gradient was less than 10–5 kcal/mol·Å. The VIBRAN utility in the CHARMM program was used to diagonalize the second derivative matrix and generate normal-mode frequencies. The harmonic approximation neglects the effects of anharmonicity in the potential energy surface. The entropy arising from hopping between different energy minima is also not accounted for by the normal-mode analysis.

To semiquantitatively estimate the anharmonic nature of the energy surface, we calculate the vibrational entropy using the quasi-harmonic approximation (QH). The QH method and its variants have been widely used for studying the dynamics of proteins and nucleic acids. For example, recently it has been used to explain the thermodynamic basis for the cooperativity of molecular association in a drug–DNA system⁴⁵ and in glycopeptide antibiotics.⁴⁶ The QH approach was first proposed for estimating the configurational entropy

difference for two conformers of a flexible molecule⁴⁷ and has been extended over the years.^{48–52} The original method used internal coordinates because of the singularity of the covariance matrix in Cartesian space.^{47,48,52} Schlitter proposed a heuristic formula which provides an upper bound for the quasi-harmonic entropy⁵⁰ while elegantly circumventing the need to use internal coordinates. Recently, Andricioaei and Karplus⁵¹ have shown that the quasi-harmonic analysis can be directly performed to calculate entropy from the Cartesian-coordinates covariance matrix, without conversions to internal coordinates or the use of a heuristic formula. The calculation of QH entropy in the present work is based on their analysis.⁵¹ In the QH approach, the configuration probability distribution is a multivariate Gaussian, i.e. $P(x) \propto \exp[-1/2(x - \langle x \rangle)^T \sigma^{-1}(x - \langle x \rangle)]$, where the covariance matrix $\sigma_{ij} = \langle (x_i - \langle x_i \rangle)(x_j - \langle x_j \rangle) \rangle$ is accumulated along a molecular dynamics trajectory. The form of $P(x)$ may be compared with the probability distribution in the canonical ensemble, i.e. $P(x) \propto \exp(-E(x)/kT)$. This comparison suggests that the effective potential is a quadratic function of coordinates $E(x) = 1/2 x^T F x$, with the effective force matrix $F = kT\sigma^{-1}$. Following the standard normal-mode procedure, the mass-weighted covariance matrix $\sigma' = M^{1/2}\sigma M^{1/2}$ is diagonalized to obtain the eigenvalues λ_i and hence the quasi-harmonic frequencies $\nu_i = 1/2\pi \sqrt{kT/\lambda_i}$. The quasi-harmonic entropy was calculated from the $3N-6$ internal quasi-harmonic modes by substituting ν_i into the vibrational entropy formula for harmonic oscillators eq 6.

The VIBRAN module in CHARMM was used to perform the quasi-harmonic analysis in this study. The covariance matrix σ_{ij} is accumulated from the molecular dynamics trajectory recorded at time intervals of 1 ps. To focus on configurational entropy due to internal motions, the global translation and rotation were removed from the dynamics trajectory prior to the quasi-harmonic analysis, by fitting each coordinate set of the trajectory to a reference structure. The snapshot at the middle point of the trajectory was chosen as a reference structure for the translational and rotational fitting. All the atoms were used in the superposition with mass weighting. We noted that for flexible molecules the rotation and the internal motions cannot be unambiguously separated.

The quasi-harmonic method was originally developed for molecular systems with a single highly populated energy well and has been shown to overestimate vibrational entropy in complex systems with multiple energy minima.⁵³ Its utility has been limited by the following factors. First, the QH entropy usually does not converge in nanoseconds MD simulations.^{28,46} Second, the assumption of multivariate normal distribution may be inadequate for describing the dynamics of flexible molecules. In the present study, we employ the QH method to obtain qualitative information regarding the relative chain flexibilities of the three secondary structural forms.

Replica-Exchange Molecular Dynamics. The rugged free energy surface in proteins and nucleic acids often causes MD simulations to be trapped in local minima. The replica exchange molecular dynamics (REMD) and similar methods have been developed to improve the efficiency of barrier crossing and conformational sampling in such situations.^{54,55}

Table 1. RNA Simulations in Explicit Water^a

name	temp (K)	starting conformation	length (ns)
D276	276	duplex	5
L276A	276	hairpin	10
L276B ^b	276	hairpin	10
S276	276	single strand	5
D300	300	duplex	5
L300	300	hairpin	70
S300	300	single strand	100

^a Unless specified, all residues in the initial structures have the C3'-endo sugar pucker. ^b The sugar pucker configuration in the initial structure is as follows: U5 and U7 have the C2'-endo pucker, while U4 and U6 are in the C3'-endo pucker.

In this approach, a simulated replica system has a finite probability of escaping local minima by exchanging its configuration with another replica simulated at a higher temperature. The Metropolis criteria governing the configuration exchange ensures that the Boltzmann distribution as a function of temperature is preserved.

Performing REMD simulation in explicit solvent is possible but computationally expensive, requiring a large number of replicas to cover a small range of temperature values. In the present study, the REMD simulation is performed for RNA hairpin conformer in a continuum solvent described by a generalized Born model with a switching (GBSW) method.^{35,36} Molecular surface was used to approximate a smoothed dielectric boundary. The nucleic acids atomic radii set derived by Banavali and Roux⁴³ for the CHARMM27 parameters was used as the input atomic radii for the GBSW method. No explicit counterions were used in the REMD simulations in continuum solvent, and the salt effect was approximated by assigning a salt concentration of 0.15 M in the GBSW method. The temperature range from 270 to 550 K was covered by 19 exponentially spaced replicas. The configuration exchange between replicas at neighboring temperatures was attempted every 2 ps. The total simulation length was 8.3 ns, and conformations generated in the last 6.3 ns were used in the analysis. The integration time step was 2 fs, and the bond lengths involving hydrogen atoms were constrained by the SHAKE method.⁵⁶ The temperature was kept at the constant value by the Nose-Hoover method.⁵⁷

3. Results and Discussion

To probe the conformational dynamics of the UUUU tetraloop 5'-CGC(UUUU)GCG-3', we performed a series of MD simulations at 276 and 300 K, initiated from duplex, hairpin, and single stranded forms. The conditions of these simulations are described in Table 1. The main results of the free energies obtained by postprocessing the molecular dynamics trajectories using the MM-PB/SA method are collected in Tables 2–5 and in Table S1 of the Supporting Information.

The free energy results presented here indicate that at low temperatures the duplex and hairpin are in equilibrium. Higher temperature destabilizes the duplex, and the hairpin become the dominant form at 300 K. Increasing the salt concentration was found to stabilize the duplex form, as would be expected from increased charge screening. Our results obtained from the normal-mode analysis and quasi-

Table 2. Free Energy Differences: (a) $T = 276$ K^{a,h} and (b) $T = 300$ K^a

	duplex - hairpin	hairpin - sst	duplex - sst ^b
(a) $T = 276$ K			
$\Delta < E(\text{intra}) >$	0.4	-1.7	-1.3
$\Delta < E(\text{elec}) >$	709.0	51.6	760.6
$\Delta < E(\text{vdw}) >$	3.0	-18.6	-15.6
$\Delta < E(\text{PB}) >^e$	-711.5	-55.2	-766.7
$\Delta < E(\text{total_elec}) >^c$	-2.5	-3.6	-6.1
$\Delta < G(\text{np}) >$	-0.6	-1.8	-2.4
$\Delta < G(\text{MM-PB/SA}) >^d$	0.3	-25.7	-25.4
$-T\Delta < S(\text{vib}) >^f$	-3.4	1.6	-1.8
$-T\Delta < S(\text{trans}) >$	6.2	0.0	6.2
$-T\Delta < S(\text{rot}) >$	5.6	0.4	5.9
$\Delta < G(\text{tot}) >^g$	8.6	-23.7	-15.1
(b) $T = 300$ K			
$\Delta < E(\text{intra}) >$	1.3	6.5	7.8
$\Delta < E(\text{elec}) >$	784.6	6.9	791.5
$\Delta < E(\text{vdw}) >$	2.7	-14	-11.3
$\Delta < E(\text{PB}) >^e$	-774.3	-22.3	-796.6
$\Delta < E(\text{total_elec}) >^c$	10.3	-15.4	-5.1
$\Delta < G(\text{np}) >$	-1.1	-1.1	-2.2
$\Delta < G(\text{MM-PB/SA}) >^d$	13.2	-24.0	-10.8
$-T\Delta < S(\text{vib}) >^f$	-3.7	0.3	-3.4
$-T\Delta < S(\text{trans}) >$	6.7	0.0	6.7
$-T\Delta < S(\text{rot}) >$	6.1	0.2	6.3
$\Delta < G(\text{tot}) >^g$	22.3	-23.5	-1.2

^a Energies are in kcal/mol, per RNA strand. ^b The label sst stands for single stranded form. ^c The total electrostatic energy $E(\text{total_elec})$ equals the sum of solute electrostatic energy $E(\text{elec})$ and the electrostatic solvation free energy $E(\text{PB})$, i.e. $< E(\text{total_elec}) > = < E(\text{elec}) > + < E(\text{PB}) >$. ^d $< G(\text{MM-PB/SA}) > = < E(\text{gas}) > + < G(\text{solv}) >$. See also eqs 2 and 3 in the text. ^e Salt concentration equals to 0.15 M. ^f $-TS(\text{vib})$ is the vibrational entropy contribution as computed by the normal-mode analysis. ^g $G(\text{tot}) = G(\text{MM-PB/SA}) - TS(\text{trans}) - TS(\text{rot}) - TS(\text{vib})$. ^h The results for the hairpin simulation were calculated using the L276A trajectory described in Table 1.

Table 3. $G(\text{MM-PB/SA})$ Free Energy Differences as a Function of Salt Concentration^a

salt concn (M)	duplex - hairpin	hairpin - sst ^b	duplex - sst ^b
0.15	0.3	-25.7	-25.4
0.01	4.6	-25.3	-20.7
0	8.6	-25.1	-16.5

^a Calculated at $T = 276$ K. Units are in kcal/mol. ^b Label sst stands for single stranded RNA.

Table 4. Vibrational Entropy Contribution $-TS(\text{QH})$,^a as Calculated by Quasi-harmonic Analysis with Different Trajectory Lengths at 276 K

length (ns)	duplex	hairpin	sst ^b	duplex - hairpin	hairpin - sst ^b
1	-214.5	-206.5	-238.7	-8.0	32.2
2	-232.6	-215.6	-256.5	-17.0	40.9
3	-243.6	-229.6	-268.4	-14.0	38.8
4	-250.7	-234.0	-291.8	-16.7	57.8
5	-260.0	-234.4	-303.0	-25.6	68.6

^a Units in kcal/mol. ^b Label sst stands for single stranded RNA.

harmonic analysis suggest that the duplex form exhibits larger vibrational entropy than the hairpin. The conformational behavior of the UUUU tetraloop may be compared with that of the more common UUCG tetraloop.¹³ Using the MM-

Table 5. Effect of Loop Residues U5/U7 Sugar Pucker on the G(MM-PB/SA) Free Energy Observed in the L276B Trajectory^a

	<i>E</i> (intra)	<i>E</i> (elec)	<i>E</i> (vdw)	<i>E</i> (PB)	<i>E</i> (total_elec)	<i>G</i> (np)	<i>G</i> (MM-PB/SA)
2–4 ns	683.6	−150.0	44.0	−1687.9	−1837.9	12.5	−1097.8
7.5–10 ns	680.9	−153.6	35.3	−1680.8	−1834.4	12.6	−1105.6

^a During the L276B simulation, both U5 and U7 are in the C2'-endo conformation between 2 and 4 ns. Transitions to the C3'-endo pucker occur at 4 ns for the U7 residue, and at 6.75 ns for the U5 residue. The whole structure remains in the stable hairpin loop conformation from 7.2 ns until the end of the trajectory. See also Figures 6–8.

PB(GB)/SA approach, Srinivasan et al. calculated the free energy of the duplex/hairpin for a 12-nucleotide UUCG tetraloop at a single temperature (300 K) and found that the hairpin was slightly more stable than the duplex at 0.1 M salt.¹³ The solute vibrational entropy was calculated using the normal-mode analysis. The vibrational entropy change $T\Delta S(\text{vib})$ was found to favor duplex over hairpin by −8.7 kcal/mol at 300 K, which is somewhat larger than the $T\Delta S(\text{vib})$ of −3.7 kcal/mol for the duplex-hairpin conversion in the 10-nucleotide UUUU tetraloop in the present study. The overall duplex/hairpin equilibrium in RNA tetraloops appears to be not strongly sensitive to the details of the loop sequence.

Free Energy Results: Neglecting Solute Entropy Contributions. The estimation of the solute entropy contribution to conformational change remains a difficult aspect in the end-point free energy methods, such as the MM-PB/SA approach.⁵⁸ Uncertainties may arise from the simple approximations used to estimate separately the translational, rotational, and vibrational entropic contributions. In several MM-PB/SA applications, only the vibrational entropy term is estimated, usually based on the normal-mode analysis. In the following, we first analyze the free energy contributions excluding the solute entropic part and later discuss the influence of entropy on the conformational equilibrium.

Table 2 summarizes the results of free energy difference calculated at 0.15 M salt concentration using the trajectories described in Table 1 (see also Table S1, Supporting Information). In each case, the calculated free energy components have been averaged over 200 snapshots for the last 2 ns of the trajectory and reported as values per single chain of RNA.

To verify the convergence of the results, we have also calculated the free energies for the last 4 ns of the simulation and using 2000 snapshots from the trajectories (Tables S2 and S3 in the Supporting Information). While the calculated $\Delta G(\text{tot})$ can differ by up to 4 kcal/mol using different trajectory data sets, these variations in $\Delta\langle G(\text{tot})\rangle$ are still small compared with the absolute values of $\Delta\langle G(\text{tot})\rangle$, which indicate that the calculated free energy components (excluding entropy contribution, as discussed below) have converged during the simulations.

Neglecting the solute entropic contributions, the total free energy for each conformational state is represented by the term $G(\text{MM-PB/SA}) = E(\text{gas}) + G(\text{soln})$ in Table S1 of the Supporting Information. As shown in Table 2(a),(b), the free energy of the hairpin is −0.3 kcal/mol and −13.2 kcal/mol more favorable than that of RNA duplex at 276 and 300 K, respectively. Both duplex and the hairpin are more stable than the single stranded form at 276 and 300 K. The results indicate that (1) hairpin and duplex are the predominantly

populated states at 276 K, and (2) the duplex structure becomes less stable and the conformational equilibrium is shifted in favor of hairpin and single stranded RNA with increasing temperature.

We compare these results with NMR spectroscopy and thermodynamic measurements. Fürtig et al.⁸ monitored the temperature-dependent NMR spectra change in this RNA. They observed signals from both hairpin and duplex at 3 °C, whereas only the hairpin signal was detected at 27 °C. They also observed that between 37 °C and 67 °C the hairpin melts and forms single stranded RNA. This trend in the temperature-induced secondary structural changes is consistent with our free energy calculations using the *G*(MM-PB/SA) approach.

Analyzing the energy components in Table S1 of the Supporting Information, we found that the total electrostatic energy *E*(total_elec) is the principal factor responsible for a favorable change in the *G*(MM-PB/SA) free energy for the hairpin over the duplex and the single stranded form. As the temperature is increased from 276 to 300 K, *E*(total_elec) becomes less negative for both the duplex and the single stranded form by ~10 kcal/mol and ~9 kcal/mol, respectively, while the *E*(total_elec) of the hairpin becomes more negative by −2.7 kcal/mol. This effect is mainly due to the fact that the favorable change in the electrostatic solvation free energy *E*(PB) of the duplex form is cancelled out by the unfavorable changes in the solute electrostatic interaction energies *E*(elec) as the temperature is raised.

These results suggest that the conformational equilibrium in the RNA hairpin studied here will be sensitive to changes in the solvent dielectric properties. The free energy results calculated at different salt concentrations are presented in Table 3, which shows that the duplex formation is favored by added salt. This prediction is supported by the experimental observation in the NMR study of the conformational equilibrium of the RNA hairpin by Fürtig et al.⁸ They found out that the signal from duplex RNA appears when the NaCl concentration is increased from 10 to 120 mM. The stabilization of the duplex is attributed to the increased charge screening by added salt in the net repulsive electrostatic interaction between the two chains in a duplex RNA. As observed in earlier studies,²³ conformers with stronger gas-phase electrostatic energy are affected by the charge screening more than those conformers with weaker electrostatic interactions, as is the case with the hairpin and single stranded forms.

The thermodynamic parameters for the hairpin formation in a 12-nucleotide GGAC(UUUU)GUCC tetraloop sequence were reported by Antao and Tinoco⁶ and more recently by Proctor and co-workers.⁷ The value of ΔH° was found to be

between -38.7 and -42.7 kcal/mol. In order to estimate the ΔH° between the hairpin and the single stranded RNA from our MM-PB/SA calculations, we excluded the solute entropy and the small nonpolar contribution $\Delta G(\text{np})$ from the MM-PB/SA free energy difference, since the latter is mainly related to changes in solvent entropy (the hydrophobic effect). This yields calculated ΔH° values between -23.9 kcal/mol at 276 K and -22.9 kcal/mol at 300 K for the equilibrium between the hairpin and the single stranded form. This result, which was obtained for the 10-nucleotide CGC-(UUUU)GCG tetraloop, is in qualitative agreement with the experimental value for the 12-nucleotide RNA hairpin.

Free Energy Results: Including Solute Entropy Contributions. The results for the total free energy difference $\Delta G(\text{tot})$, which includes the solute translational, rotational entropies, and the normal modes entropy $T\langle S(\text{vib}) \rangle$, are presented in Table 2 (see also Table S1 in the Supporting Information). The values for the $\Delta G(\text{tot})$ between the hairpin and the duplex are -8.6 and -22.3 kcal/mol at 276 and 300 K, respectively, while the $\Delta G(\text{tot})$ between duplex and the single stranded RNA is -15.7 kcal/mol at 276 K and -1.2 kcal/mol at 300 K. These results are qualitatively consistent with a shift in the conformational preferences favoring the hairpin and single stranded form over the duplex as the temperature is increased.

As expected, the translational/rotational entropy terms are found to oppose the duplex formation. The normal-mode analysis gives similar vibrational entropy contributions for the three secondary structural forms. At 276 K, the duplex has a slightly more favorable $T\langle S(\text{vib}) \rangle$ than the hairpin and the single stranded RNA by -3.5 and -1.8 kcal/mol, respectively. This result reflects that on average the duplex RNA exhibits larger vibrational motions, possibly due to the four mismatched U–U base pairing in the middle of the double helices. The small differences in the $T\langle S(\text{vib}) \rangle$ also suggest that the energy landscape for local minima is largely dependent on the topology, i.e., atom connectivity determined by bond, angles, and torsions which are similar for the three structural forms, with some modulation by the presence and the strength of the nonbonded interactions such as hydrogen bonds.

Our calculations predict a $\Delta G(\text{tot})$ of -8.6 kcal/mol for the hairpin-duplex equilibrium at 276 K in favor of the hairpin. However, according to the NMR study the two forms coexist at 3 °C, which means that the free energy difference $\Delta G(\text{tot})$ is expected to be small and needs to be of the order of 0 kcal/mol at 276 K. The -8.6 kcal/mol difference between the calculated $\Delta G(\text{tot})$ and the experimental $\Delta G(\text{tot})$ suggests that certain free energy contributions are missing or calculated with insufficient accuracy. We think that this can be partially attributed to the inadequacy of the harmonic analysis in estimating the conformational entropy.

In this context we examined approximations that are used in calculation of the solute entropy. While the vibrational entropy evaluated using the harmonic analysis favors the duplex form over the hairpin by about 3.5 kcal/mol, the calculation using normal-mode analysis does not capture the changes in conformational entropy associated with transitions between energy minima. This view is qualitatively supported

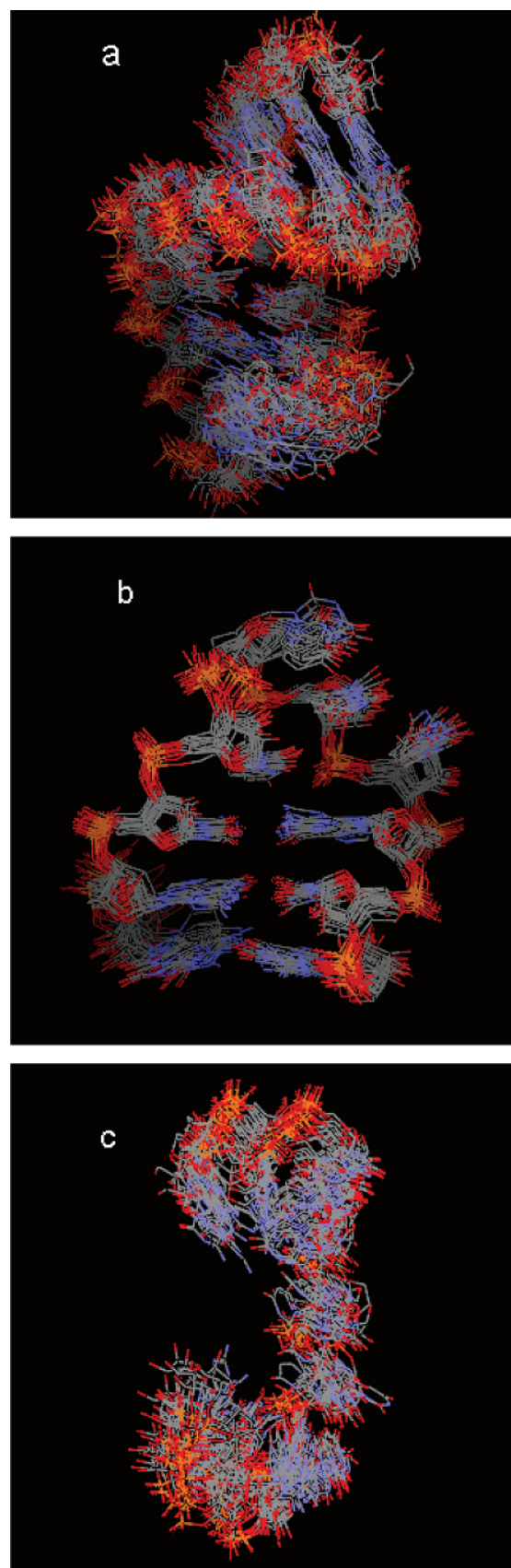


Figure 2. Superimposed snapshots from the trajectories obtained at 276 K: (a) duplex, (b) hairpin, and (c) single stranded form.

by the overlay of the superimposed RNA structures presented in Figure 2, which shows that the duplex form is considerably

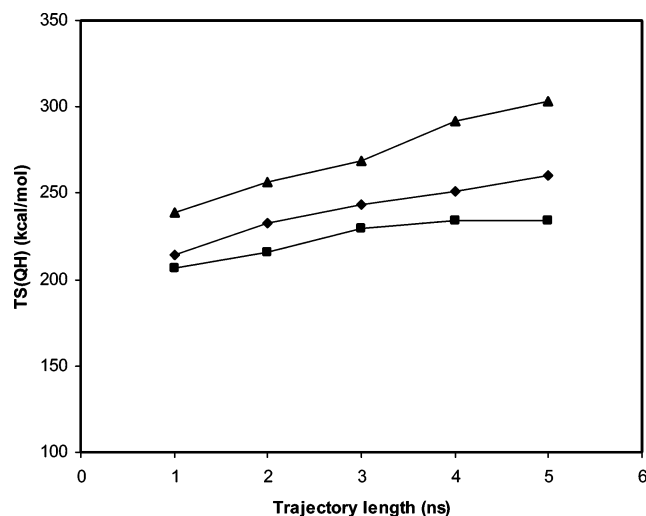


Figure 3. Quasi-harmonic entropy contributions TS(QH) calculated at 276 K for different lengths of the MD trajectories: single strand (triangle), duplex (diamond), and hairpin (square).

more flexible than the hairpin. This suggests that conformational entropy $\Delta S(\text{conf})$ favors the duplex formation. Figure 2 also shows that the single stranded RNA is more disordered than both the duplex RNA and the hairpin form, which suggests that the rank order of the solute conformational entropy is $S(\text{single strand}) > S(\text{duplex}) > S(\text{hairpin})$.

Interestingly, the trend in relative conformational entropy for the three secondary structural forms is reproduced by the quasi-harmonic calculation of entropy: see Table 4 and Figure 3 for the results of TS(QH) calculated from different trajectory lengths. Although the calculated quasi-harmonic entropy did not converge within 5 ns of sampling, the rank order of the relative vibrational entropy clearly indicates that $S(\text{single strand}) > S(\text{duplex}) > S(\text{hairpin})$, which is consistent with the general picture of conformational fluctuation shown in Figure 2. The trend of relative vibrational entropy remains unchanged with the length of trajectory segment used in calculating TS(QH).

However, it can be shown that the calculated $T\Delta S(\text{QH})$ is significantly overestimated relative to expected values. We use the data set obtained with the 2 ns trajectory segment to illustrate this point. The calculated $T\Delta S(\text{QH})$ between the duplex RNA and hairpin is -8.4 kcal/mol more negative than the -8.6 kcal/mol required to bring the calculated $\Delta G(\text{tot})$ for the duplex-hairpin equilibrium to the experimental value of 0 kcal/mol at 276 K. The quasi-harmonic entropy are overestimated even more for the single stranded RNA: including the $T\Delta S(\text{QH})$ calculated for the 2 ns trajectory segment in the free energy results predicts that the single stranded RNA is more stable than the hairpin by about -17.2 kcal/mol at 276 K, in contradiction to the experimental finding that the hairpin and the duplex RNA are the predominant forms at this temperature.

Two conclusions emerge from this result. First, the discrepancy between experimental and calculated $\Delta G(\text{tot})$ for the duplex/hairpin equilibrium may be qualitatively explained by the conformational entropy which is not accounted for by the simple harmonic approximation used

by the normal-mode analysis to calculate $T\Delta S(\text{vib})$ as shown in Table 2. Second, while the quasi-harmonic analysis correctly predicted the rank order of relative conformational entropy contribution, the method significantly overestimates the entropy difference for the 10-nucleotide RNA molecule. This error could be related to the assumption of a multivariate Gaussian distribution in the quasi-harmonic approximation, which does not hold in the presence of configurational transitions involving multiple energy wells.^{53,59} Clearly, more accurate treatment of the conformational entropy beyond the level of harmonic/quasi-harmonic model is required for a quantitative understanding of the duplex-hairpin equilibrium.

The larger conformational fluctuations exhibited by the duplex compared to the other forms may be attributable to the dynamics of internal loop formed by the four mismatched U–U base pairs in the center of the helix. The relative flexibility in different parts of the duplex structure can be seen from the overlay of the superimposed segment structures (Figure S4, Supporting Information). The internal loop in the duplex shows more fluctuation than the helix regions in the duplex; it is also more disordered than the loop and stem regions in the hairpin form. Fluctuation in the internal loop of the duplex is also likely to be transmitted to the two ends of the double helix and enhance the bending and twisting of the helix, although MD simulations at longer time scale is needed to observe such large scale movement. Figure S4 also suggests that the stem and the loop region of the hairpin structure have similar flexibility.

Stable Hairpin Loop Conformers Observed in Explicit Solvent Simulations. The MD simulations L276A and L300, which are initiated from hairpin conformations at 276 and 300 K, respectively, converged to the same lowest energy conformer (Figures S5 and S6, Supporting Information). In both simulations, the rms deviation relative to the final structure of the L300 simulation decreases to less than 1.5 Å. In L276A simulation, the transition to the converged structure occurs at 7.7 ns, while the similar transition occurs at a much later time, ~ 50 ns, for the L300 simulation. The transitions to the converged structure resulted in reductions in the MM-PB/SA free energy between -15 kcal/mol and -20 kcal/mol relative to the initial structure, indicating that the final structure attained by the two simulations is the most stable loop conformation described by the physical model used in the present study. Since the 3D coordinates are not available for the hairpin structure from NMR studies, we cannot rule out that our simulation starting from modeled hairpin conformations may not have converged to the global free energy minima. However, the following observations suggest that the final parts of the trajectory in our explicit solvent simulations have converged to physically viable conformational states: (1) free energies and structures stabilized in the 70 ns simulation at 300 K; (2) independent simulations at 276 and at 300 K led to the same low-energy hairpin conformations; (3) some experimental results, such as ΔH° of hairpin melting and the temperature dependence of conformational equilibrium, are reproduced reasonably well by free energy calculations using the last part of the trajectories.

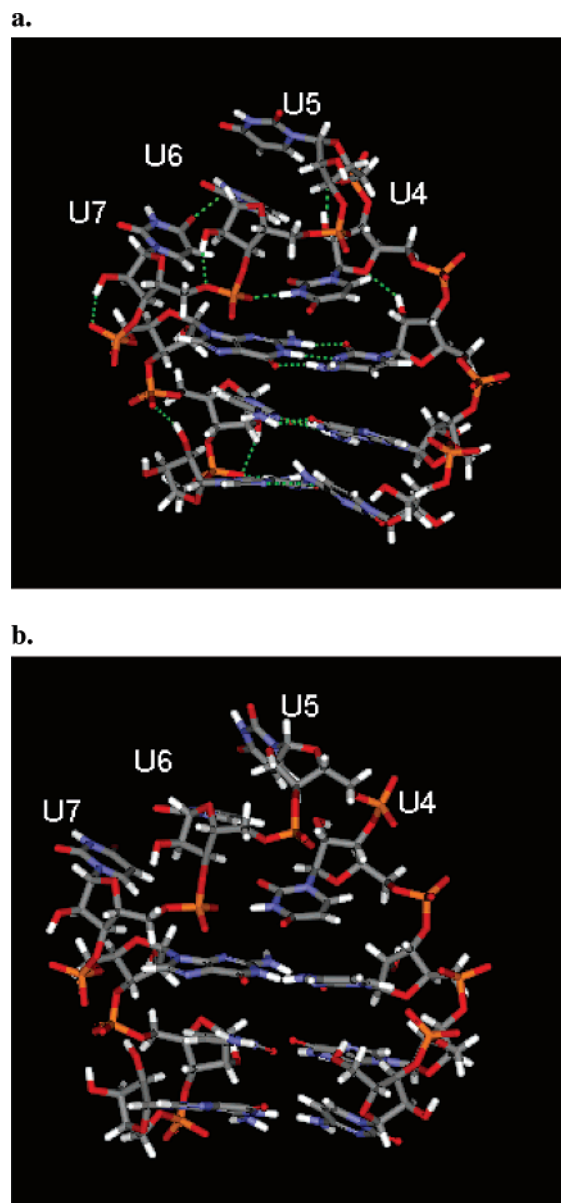


Figure 4. Final structures in the (a) L276A and (b) L300 simulations.

The final structures from the L276A and L300 trajectories are shown in Figure 4(a),(b). Several specific interactions can be identified in these structures: a weak stacking interaction between the U5 and U6, a hydrogen bond between the U4 base and the phosphate linking the U6 and U7, and hydrogen bonds involving the 2'OH groups at U4 and U6. The stacking interaction between the U5 and U6 bases is persistent for the most part of the 70 ns simulation L300 (Figure S1, Supporting Information), and the average separation distance between the U5 and U6 bases is around 4 Å. The van der Waals interaction between the U5 and U6 bases contributed about -4.0 kcal/mol to the stability of the loop. In Figure S7 of the Supporting Information, the existence of a CH...O hydrogen bond between C6-H (U7) and O5'-(U7) is highlighted (see also Figure S2 in the Supporting Information for the time dependence of this hydrogen bond). This CH...O hydrogen bond has a 73% time occupancy during the simulation (using a 3.7 Å cutoff) and is also present in the crystal structure of the 1mme hairpin loop,

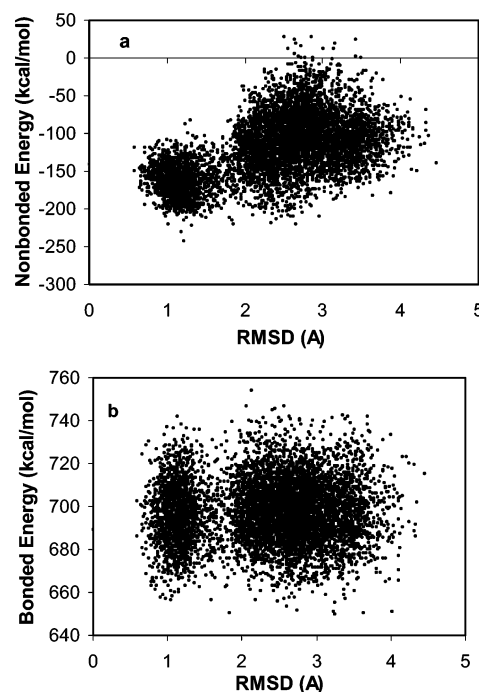


Figure 5. Free energy components in the L300 simulation: (a) total gas-phase nonbonded energy $E(\text{elec}) + E(\text{vdw})$ as a function of the rms deviation relative to the final structure and (b) total bonded energy $E(\text{intra})$ as a function of the rms deviation relative to the final structure.

from which the current UUUU hairpin is modeled. The importance of these nonbonded interactions in stabilizing the loop conformation can be seen in Figure 5(a), which shows that the conformers in the same cluster as the final structure have favorable total gas-phase electrostatic and van der Waals, $E(\text{vdw}) + E(\text{elec})$, interaction energy. In contrast to the nonbonded energy, the bonded energy term showed no correlation with the distance in rmsd space from the stable loop structure (Figure 5(b)).

Sugar Pucker Preferences. A recent NMR study⁷ on the cUUUg tetraloop found that U4 adopts the C3'-endo and U6 is 37% C2'-endo, while both U5 and U7 have predominantly the C2'-endo pucker. In the 70 ns hairpin simulation L300, which started with the four uridines in the C3'-endo conformation, conversion to the NMR sugar pucker mode did not occur, and all four uridines maintain the C3'-endo conformation throughout the simulation.

To investigate the relative stability of different sugar pucker for the loop residues, we conducted a 10 ns hairpin simulation L276B at 276 K, starting with the NMR pucker configuration in which the U4 and U6 are C3'-endo, while U5 and U7 are C2'-endo. Interestingly, in this simulation both the U5 (from 6.75 ns) and U7 (from 4 ns) are converted into the C3'-endo conformation: see Figure 6. This transition to the C3'-endo pucker is also reflected by the rmsd results for the loop residues: as seen from Figure 7, at 7.2 ns the loop conformation is converted into the stable hairpin loop structure observed in the L276A and L300 simulations. The automatic transition to the C3'-endo pucker suggests that according to the physical model used in the present study, the C3'-endo conformation is more stable than the C2'-endo conformation deduced from NMR analysis.

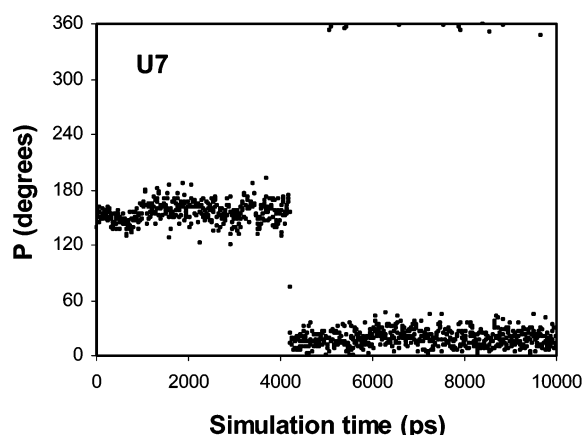
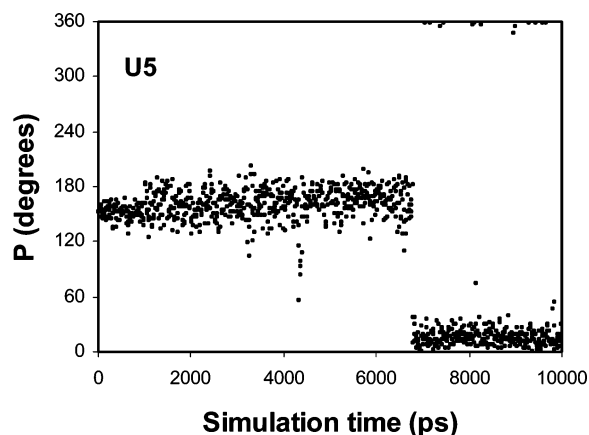


Figure 6. Results for the L276B simulation: the sugar pucker pseudorotation phase angle P for U5 and U7 as a function of simulation time.

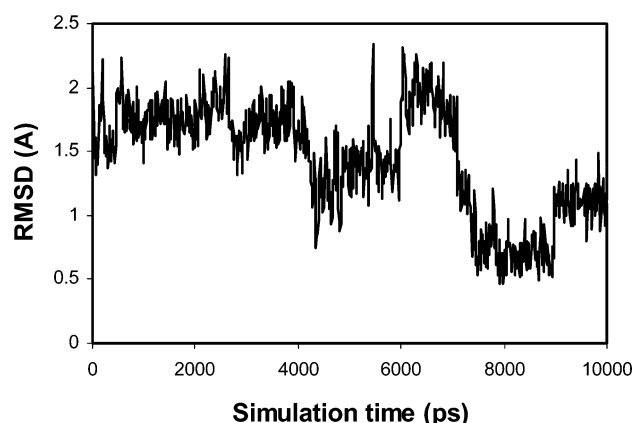


Figure 7. Results for the L276B simulation: rms deviation for the loop residue (c3-U4-U5-U6-U7-g8) relative to the last frame in the L300 trajectory as a function of simulation time. rmsd are calculated for the heavy atoms in the loop.

Two conformational substates of interest can be identified in Figure 6: the 2–4 ns time window corresponds to the C2'-endo conformer observed in the NMR study, and the 7.5–10 ns window represents the C3'-endo state. Representative structures for these two states are shown in Figure 9. These structure snapshots taken before and after the S-type \rightarrow N-type sugar pucker transition reveals that the C3'-endo conformer is stabilized by the U5–U6 and U6–U7 base stacking interactions. This base stacking is not possible to

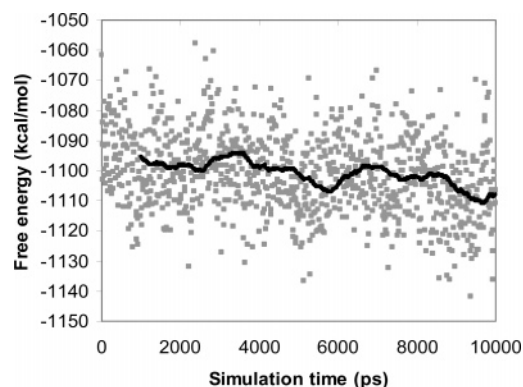


Figure 8. Results for the L276B simulation: G(MM-PB/SA) free energy as a function of simulation time.

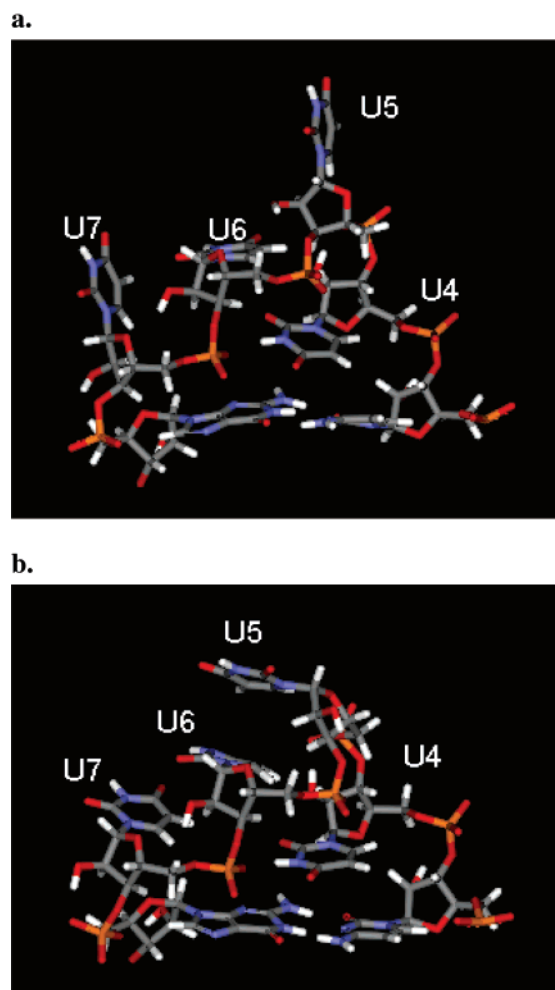


Figure 9. Results for the L276B simulation: representative structures in which both U5 and U7 are in the (a) C2'-endo and (b) C3'-endo conformations. Structures shown in (a) and (b) are from the 4 and 10 ns snapshots, respectively.

create in the C2'-endo puckering mode where the U5 and U7 bases extend out into the solvent phase.

Based on the above assignment of conformational substates, we calculated the effects of the loop sugar pucker on free energy (Table 5). The C2'-endo conformer has more favorable electrostatic solvation free energy $E(\text{PB})$, which is consistent with the fact that the U5 and U7 in the C2'-endo state extend away from the loop and thus are better

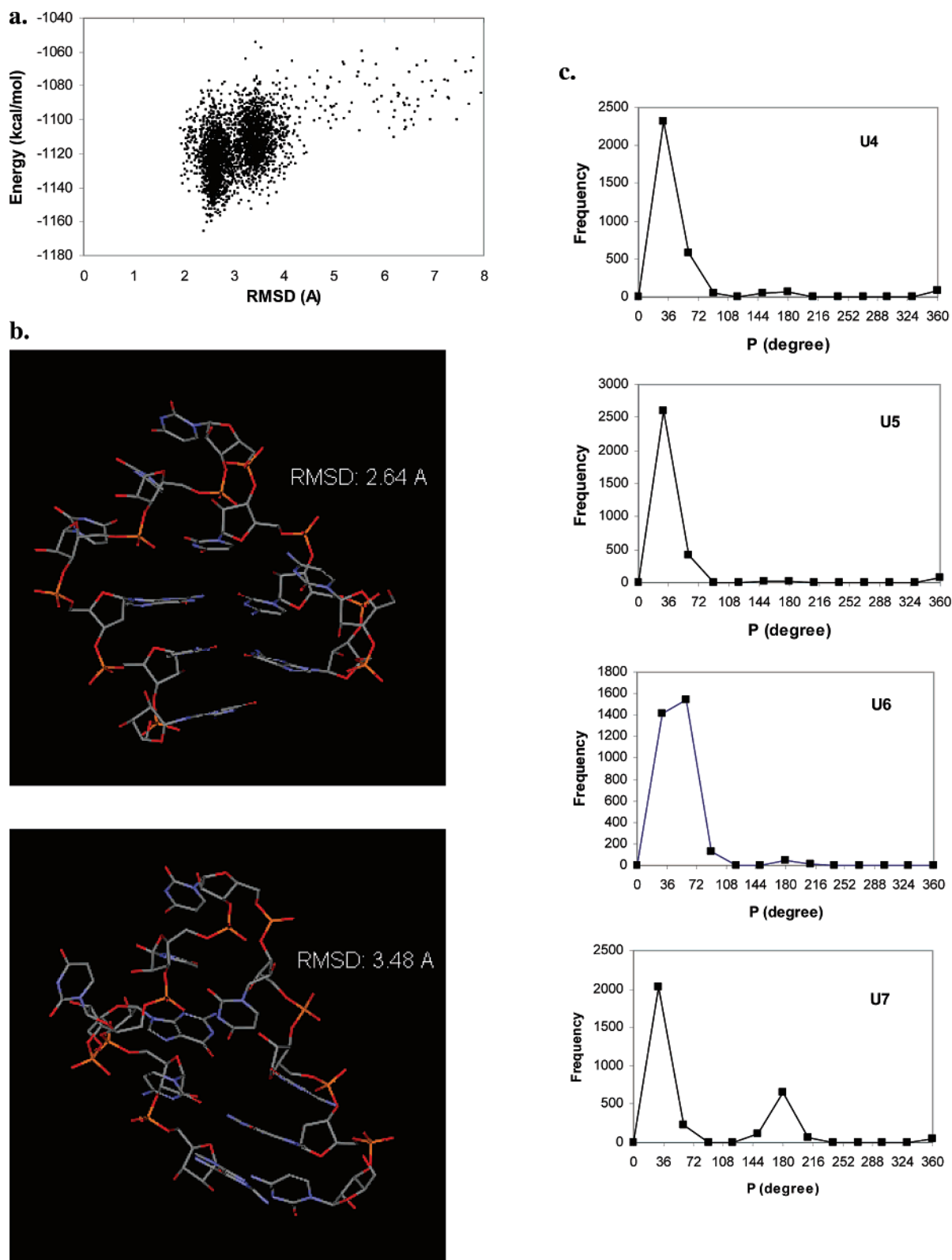


Figure 10. Results for the REMD simulation: (a) the total energy as a function of rms deviation from the starting structure, which is the stable hairpin loop conformation observed in the explicit solvent simulations, (b) representative structures for the two most populated clusters, and (c) the time occupancy of the sugar pucker modes for the four uridines. All data were collected from the last 6.3 ns of the simulation.

solvated (Figure 9). However, while the total electrostatic energy $E(\text{total_elec})$ favors the more extended conformation in Figure 9(a), this is offset by the larger unfavorable changes in the van der Waals energy and the bonded energy. The unfavorable van der Waals energy is associated with the loss

of U5–U6 and U6–U7 base stacking in the C2'-endo conformer discussed earlier. Overall, the MM-PB/SA calculation predicts that the C3'-endo is more stable than the C2'-endo structure by -8 kcal/mol (Table 5 and Figure 8), which is in discrepancy with the NMR experiments.

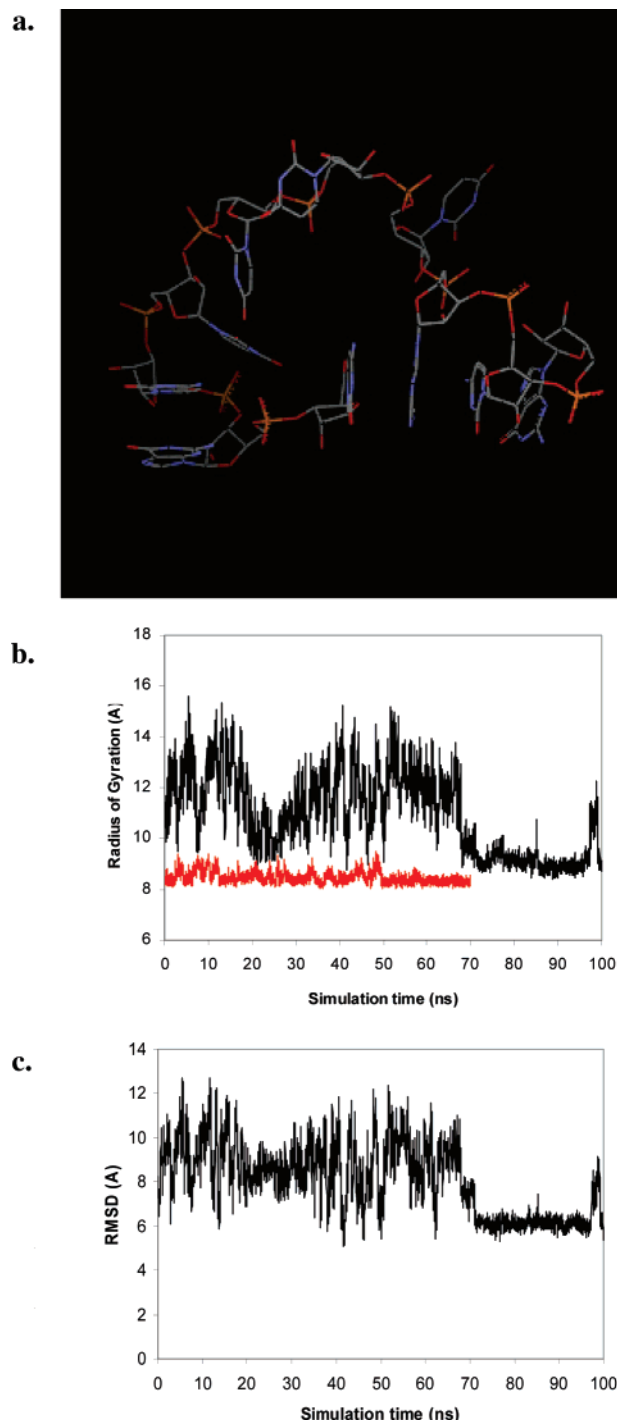


Figure 11. Results for the S300 simulation: (a) the final structure, (b) the temporal history of the radius of gyration for the S300 trajectory (black) and the L300 trajectory (red), and (c) the root-mean-squared distance (rmsd) from the hairpin loop structure as a function of the simulation time.

Although errors in the NMR data analysis cannot be completely ruled out, we think that the disagreement between our simulation and the NMR results more likely reflects some problems in the simulation method/energy model used in the explicit solvent and implicit solvent simulations in this study. Our simulation results shows that the repuckering to the experimental values was not achieved in 70 ns MD simulation in TIP3P water, although some limited repuckering is

seen from Replica-Exchange MD in the GBSW implicit solvent model (see below).

It is not clear whether the problem lies in force-field parametrization or is simply a result of limited sampling of the phase space. MacKerell⁴⁰ and co-workers reported the conformational energetics for a single deoxyribose sugar using the CHARMM27 parameter set. The energy difference between the North- and South-type sugar is <1 kcal/mol, and the barrier between the two conformations through the O4'-endo conformation is ≤ 3 kcal/mol. These values for sugar pucker in single nucleotide are consistent with estimations from ab initio calculations.²⁵

In the loop region of the RNA hairpin, where 2'-OH hydroxyl groups can interact with neighboring nucleotide, ions and water, the barrier between the N- and S-type sugar pucker should be higher than those in the single deoxyribose. This may explain sampling problem in our calculations, where the repuckering to the experimental values was not achieved in 70 ns MD in TIP3P water. The fact that some limited repuckering is seen from our REMD simulations in the GBSW implicit solvent model reflects the role of solvent molecules in slowing down the conformational dynamics.

In addition to possible problems with the potential energy function used in the MD simulations, the MM-PB/SA scoring method may not be accurate or sensitive enough to correctly rank the different conformations of a few ribose moieties in the loop region: the MM-PB/SA calculation actually favors the hairpin conformer observed in MD simulation, which exhibits the non-NMR sugar pucker. This incorrect result underscores the limitation of MM-PB/SA discussed in the Introduction.

We feel that a more thorough study is warranted to clarify the situation on the stability and the energy barrier of conversion in ribose conformation in RNA hairpin, and such a study should be useful for improving force field and implicit solvent model.

Replica Exchange MD Simulations. We performed replica exchange MD simulation to explore broader conformational space for the hairpin form. The REMD simulation was initiated from the stable loop conformation obtained in the explicit solvent simulations. The results presented in Figure 10(a) reveal a funnel-like energy surface and a clear correlation between the total energy and the rmsd from initial structure. The low rmsd conformers are associated with low MM-GBSA energy, indicating that the stable hairpin conformation observed in the explicit solvent simulation corresponds to the free energy minimum. Two most populated clusters are identified in Figure 10(a), and their representative structures are shown in Figure 10(b). In the low rmsd structure (Figure 10(b)), the loop conformation is close to the initial structure, and the rmsd of 2.64 Å arises mainly from the base pair fraying at the end of the stem. Excluding the two end residues, the rmsd is 1.54 Å.

Interestingly, in the high rmsd structure in Figure 10(b), the U7 sugar exhibits the C2'-endo pucker, in agreement with the NMR sugar puckering. This high rmsd structure shows more distortions in both the loop and the stem, and as seen from Figure 10(a), it is thermodynamically less stable than the low rmsd structure by ~ 10 kcal/mol. Thus, in agreement

with our explicit solvent simulations, the REMD simulations also indicate that the C3'-endo conformation is preferred over the C2'-endo form for U7 sugar.

Figure 10(c) shows the time occupancies of the sugar pucker pseudorotation phase angle for the four uridines. While the U4, U5, and U6 sugar rings are predominantly in the C3'-endo conformation, the REMD simulation revealed more variations in the sugar pucker of the U7 ribose ring, in which the ratio between the time occupancy for the C2'-endo and that for the C3'-endo conformations is 1:2.7. It should be noted that while the REMD simulation reveals the trend in the conformational flexibility of the loop residues, the sampling is limited by the duration of the simulation length, and the results may not reflect the true equilibrium condition.

Submicrosecond Simulation of Single Stranded RNA.

A 100 ns simulation initiated from the single stranded conformation was performed at 300 K in an explicit water solvent to study a possible folding pathway for the formation of hairpin loop. As seen from Figure 11, although the RNA did not fold into the nativelike hairpin structure during 100 ns of simulation, the transitions toward more compact structures were observed. These structures have a similar radius of gyration to that of the hairpin loop. The rmsd of the final structure is 5.8 Å from the native hairpin conformation. The structure appears to be trapped into a local minima stabilized by the incorrect base stacking between the two end nucleotides. The MM-PB/SA calculation suggests that the inability to fold the RNA into hairpinlike structures is attributable to the inadequate sampling at room temperature in explicit solvent: as can be seen from Table 2b, the average $G(\text{MM-PB/SA})$ of the single stranded RNA at the end of the 100 ns simulation is 24.0 kcal/mol higher than that of the hairpin conformations. Simulations of a much longer time scale, possibly using REMD techniques, would be needed to observe folding of the hairpin at room temperature in explicit solvent.

4. Conclusions

To investigate the physical basis for the conformational equilibrium in a 10-nucleotide UUUU RNA tetraloop, we have applied the MM-PB/SA method to estimate the free energies of different RNA secondary structures in solution. The results reproduce the experimental trend in relative stabilities of duplex, hairpin loop, and single stranded RNA at two temperatures: The difference in calculated values of the $G(\text{MM-PB/SA})$ free energy between the duplex and hairpin is close to zero at low temperature. With the increase in temperature, the duplex structure was found to be destabilized, consistent with the experiments. The calculated ΔH° for the hairpin-single strand RNA conversion falls into the range of the experimental values for similar UUUU RNA tetraloops.

While the results using the gas-phase and solvation terms in the free energy calculation reproduce the experimental enthalpy and the trend of conformational equilibrium as a function of temperature, neglecting the entropy contributions yields calculated ΔG for the hairpin-duplex RNA equilibrium

larger than the experimental values at 276 K. Qualitatively, we have shown that the three secondary structural forms exhibit significantly different conformational fluctuations, and the rank order of the solute conformational entropy is $S(\text{single strand}) > S(\text{duplex}) > S(\text{hairpin})$. We used the normal-mode analysis and quasiharmonic analysis to estimate this entropic contribution to free energy. Results from both methods indicate that the helical duplex exhibits more chain flexibility than the hairpin, in agreement with inspection of the geometry fluctuations in the snapshots extracted from the trajectory. The quasiharmonic method reproduces the ranking order for the relative conformational flexibility, but the calculated entropies are overestimated. Overall, the quantitative estimation of entropy remains a very challenging task and is the major source of the uncertainties in the free energy determination using end-point methods such as the MM-PB/SA approach.

Our simulations conducted at two temperatures revealed the low-energy hairpin loop structure and a number of specific interactions that are responsible for its stability. However, the predicted sugar pucker modes in the U5 and U7 loop uridines in the low-energy hairpin conformation are different from those suggested from NMR experiments. This inability to reproduce the experimental sugar pucker mode for the two loop uridines suggests that either the experimental data are not precise enough or there are flaws in the simulation protocol adopted here. Accuracies in MD simulations are known to be limited by errors in the force-field parametrization and inadequate sampling of the configuration space. The importance of more extensive sampling was underscored by our 8.3 ns REMD simulation in the GBSW continuum solvent initiated from the hairpin loop structure.

Although the REMD simulation confirmed the stability of the low-energy loop structure observed in the explicit solvent simulations, it reveals significantly more fluctuation in the sugar pucker of the U7 ribose ring, and the results of the time occupancies for the C3'-endo and C2'-endo conformations are in better agreement with the experimental values compared to those predicted from the explicit solvent simulations. Using advanced sampling methods such as REMD at a longer time scale combined with more accurate implicit solvent models could eventually improve the theoretical results.

Acknowledgment. We thank Dr. Jianhan Chen for helpful discussions. We also thank Dr. Jayashree Srinivasan for providing the reprint of ref 13.

Supporting Information Available: Three tables and figures. The free energy results obtained at $T = 276$ K and $T = 300$ K; the free energy differences $\Delta \langle G(\text{tot}) \rangle$ calculated using different trajectory segments; the free energies calculated using different coordinate sets along MD trajectories; the distance between the U5 and U6 bases in the L300 simulation; the distance between C6 (U7) and O5' (U7) as a function of simulation time in the L300 simulation; MM-PB/SA free energy as a function of simulation time at 276 K; the superimposed structures for different parts of the

RNA; the results for the L300 and L276 trajectories: RMSD from the last frames of the trajectories and MM-PBSA calculations; the CH \cdots O hydrogen bond between C6H (U7) and O5' (U7); and the starting and final conformations of the different secondary structural forms from simulations. This material is available free of charge via the Internet at <http://pubs.acs.org>.

References

- (1) Uhlenbeck, O. Nucleic-acid structure-tetraloops and RNA folding. *Nature* **1990**, *346*, 613–614.
- (2) Jagath, J. R.; Matassova, N. B.; de Leeuw, E.; Wernecke, J. M.; Lentzen, G.; Rodnina, M. V.; Lührink, J.; Wintermeyer, W. Important role of the tetraloop region of 4.5S RNA in SRP binding to its receptor FtsY. *RNA* **2001**, *7*, 293–301.
- (3) Althoff, S.; Selinger, D.; Wise, J. A. Molecular evolution of SRP cycle components: Functional implications. *Nucleic Acids Res.* **1994**, *22*, 1933–1947.
- (4) Antao, V. P.; Lai, S. Y.; Tinoco, I., Jr.; A thermodynamic study of unusually stable RNA and DNA hairpins. *Nucleic Acids Res.* **1991**, *19*, 5901–5905.
- (5) Persson, T.; Hartmann, R. K.; Eckstein, F. Selection of hammerhead ribozyme variants with low Mg²⁺ requirement: importance of stem-loop II. *ChemBioChem* **2002**, *3*, 1066–71.
- (6) Antao, V. P.; Tinoco, I., Jr. Thermodynamic parameters for loop formation in RNA and DNA hairpin tetraloops. *Nucleic Acids Res.* **1992**, *20*, 819–824.
- (7) Proctor, D. J.; Ma, H.; Kierzek, E.; Kierzek, R.; Gruebele, M.; Bevilacqua, P. C. Folding thermodynamics and kinetics of YNMG RNA hairpins: specific incorporation of 8-bromoguanosine leads to stabilization by enhancement of the folding rate. *Biochemistry* **2004**, *43*, 14004–14014.
- (8) Fürtig, B.; Richter, C.; Wöhnert, J.; Schwalbe, H. NMR spectroscopy of RNA. *ChemBioChem* **2003**, *4*, 936–962.
- (9) Cheatham, T. E. III Simulation and modeling of nucleic acid structure, dynamics and interactions. *Curr. Opin. Struct. Biol.* **2004**, *14*, 360–367.
- (10) MacKerell, A., Jr.; Nilsson, L. *Nucleic acid simulations, Computational Biochemistry and Biophysics*; Becker, O., MacKerell, A., Jr., Roux, B., Watanabe, M., Eds.; Marcel Dekker Inc.: New York, 1999; pp 441–463.
- (11) Orozco, M.; Perez, A.; Noy, A.; Luque, F. Theoretical methods for the simulation of nucleic acids. *Chem. Soc. Rev.* **2003**, *32*, 350–364.
- (12) Karplus, M.; Kuriyan, J. Molecular dynamics and protein function. *Proc. Natl. Acad. Sci.* **2005**, *102*, 6679–6685.
- (13) Srinivasan, J.; Miller, J.; Kollman, P.; Case, D. Continuum solvent studies of the stability of RNA hairpin loops and helices. *J. Biomol. Struct. Dyn.* **1998**, *16*, 671–682.
- (14) Williams, D.; Hall, K. Experimental and computational studies of the G[UUCG]C RNA tetraloop. *J. Mol. Biol.* **2000**, *297*, 1045–1061.
- (15) Sorin, E.; Engelhardt, M.; Herschlag, D.; Pande, V. RNA simulations: probing hairpin unfolding and the dynamics of a GNRA tetraloop. *J. Mol. Biol.* **2002**, *317*, 493–506.
- (16) Sarzynska, J.; Nilsson, L.; Kulinski, T. Effects of base substitutions in an RNA hairpin from molecular dynamics and free energy simulations. *Biophys. J.* **2003**, *85*, 3445–3459.
- (17) Sorin, E.; Rhee, Y.; Pande, V. Does water play a structural role in the folding of small nucleic acids? *Biophys. J.* **2005**, *88*, 2516–2524.
- (18) Sorin, E.; Rhee, Y.; Nakatani, B.; Pande, V. Insights into Nucleic Acid Conformational Dynamics from Massively Parallel Stochastic Simulations. *Biophys. J.* **2003**, *85*, 790–803.
- (19) Spackova, N.; Sponer, J. Molecular dynamics simulations of sarcin-ricin rRNA motif. *Nucleic Acids Res.* **2006**, *34*, 697–708.
- (20) Li, W.; Ma, B.; Shapiro, B. Molecular dynamics simulations of the denaturation and refolding of an RNA tetraloop. **2001**, *19*, 381–396.
- (21) Williams, D. J.; Hall, K. B. Unrestrained Stochastic Dynamics Simulations of the UUCG Tetraloop Using an Implicit Solvation Model. *Biophys. J.* **1999**, *76*, 3192–3205.
- (22) Fadrna, E.; Spackova, N.; Stefl, R.; Koca, J.; Cheatham, T. E., III; Sponer, J. Molecular dynamics simulations of Guanine quadruplex loops: advances and force field limitations. *Biophys. J.* **2004**, *87*, 227–242.
- (23) Srinivasan, J.; Cheatham, T. E., III; Cieplak, P.; Kollman, P.; Case, D. Continuum solvent studies of the stability of DNA, RNA and phosphoramidate-DNA helices. *J. Am. Chem. Soc.* **1998**, *120*, 9401–9409.
- (24) Jayaram, B.; Sprous, D.; Young, M. A.; Beveridge, D. L. Free Energy Analysis of the Conformational Stability of A and B Forms of DNA in Solution. *J. Am. Chem. Soc.* **1998**, *120*, 10629–10633.
- (25) Kollman, P. I.; Massova, I.; Reyes, C.; Kuhn, B.; Huo, S.; Chong, L.; Lee, M.; Lee, T.; Duan, Y.; Wang, W.; Donini, O.; Cieplak, P.; Srinivasan, J.; Case, D.; Cheatham, T., III Calculating structures and free energies of complex molecules: combining molecular mechanics and continuum models. *Acc. Chem. Res.* **2000**, *33*, 889–897.
- (26) Swanson, J.; Henchman, R.; McCammon, J. Revisiting free energy calculations: A theoretical connection to MM/PBSA and direct calculation of the association free energy. *Biophys. J.* **2004**, *86*, 67–74.
- (27) Zoete, V.; Meuwly, M.; Karplus, M. Study of the insulin dimerization: binding free energy calculations and per-residue free energy decomposition. *Proteins* **2005**, *61*, 79–93.
- (28) Gohlke, H.; Case, D. Converging free energy estimates: MM-PB(GB)SA studies on the protein-protein complex Ras-Raf. *J. Comput. Chem.* **2004**, *25*, 238–250.
- (29) Jayaram, B.; McConnell, K.; Dixit, S.; Beveridge, D. Free Energy Analysis of Protein–DNA Binding: The EcoRI Endonuclease–DNA Complex. *J. Comput. Phys.* **1999**, *151*, 333–357.
- (30) Spackova, N.; Cheatham, T. E., III; Ryjáček, F.; Lankas, F.; van Meervelt, L.; Hobza, P.; Sponer, J. Molecular Dynamics Simulations and Thermodynamics Analysis of DNA-Drug Complexes. Minor Groove Binding between 4',6-Diamidino-2-phenylindole and DNA Duplexes in Solution. *J. Am. Chem. Soc.* **2003**, *125*, 1759–1769.

- (31) Gouda, H.; Kuntz, I.; Case, D.; Kollman, P. Free energy calculations for theophylline binding to an RNA aptamer: Comparison of MM-PBSA and thermodynamic integration methods. *Biopolymers* **2003**, *68*, 16–34.
- (32) Lee, M.; Duan, Y.; Kollman, P. Free energy analysis of the folding process of villin headpiece subdomain. *Proteins* **2000**, *39*, 309–316.
- (33) Cubero, E.; Luque, F.; Orozco, M. Theoretical studies of d (A:T)-based parallel-stranded DNA duplexes. *J. Am. Chem. Soc.* **2001**, *123*, 12018–12025.
- (34) Spackova, N.; Berger, I.; Spomer, J. Nanosecond molecular dynamics of zipper-like DNA duplex structures containing sheared G:A mismatch pairs. *J. Am. Chem. Soc.* **2000**, *122*, 7564–7572.
- (35) Im, W.; Lee, M. S.; Brooks, C. L., III Generalized born model with a simple smoothing function. *J. Comput. Chem.* **2003**, *24*, 1691–1702.
- (36) Lee, M. S.; Salsbury, F. R., Jr.; Brooks, C. L., III Novel generalized Born methods. *J. Chem. Phys.* **2002**, *116*, 10606–10614.
- (37) Scott, W. G.; Finch, J. T.; Klug, A. The crystal structure of an all-RNA hammerhead ribozyme: a proposed mechanism for RNA catalytic cleavage. *Cell* **1995**, *81*, 991–1002.
- (38) Jorgensen, W. L.; Chandrasekhar, J.; Madura, J.; Impey, R. W.; Klein, M. L. Comparison of simple potential functions for simulating liquid water. *J. Chem. Phys.* **1983**, *79*, 926–935.
- (39) Brooks, B.; Bruccoleri, R.; Olafson, B.; States, D.; Swaminathan, S.; Karplus, M. CHARMM: A program for macromolecular energy, minimization, and dynamics calculations. *J. Comput. Chem.* **1983**, *4*, 187–217.
- (40) Foloppe, N.; MacKerell, A. D., Jr. All atom empirical force field for nucleic acids: 1) Parameter optimization based on small molecule and condensed phase macromolecular target data. *J. Comput. Chem.* **2000**, *21*, 86–104.
- (41) MacKerell, A., Jr.; Banavali, N. All-atom empirical force field for nucleic acids: 2) Application to molecular dynamics simulations of DNA and RNA in solution. *J. Comput. Chem.* **2000**, *21*, 105–120.
- (42) Essmann, U.; Perera, L.; Berkowitz, M. L.; Darden, T.; Lee, H.; Pedersen, L. A smooth particle mesh Ewald method. *J. Chem. Phys.* **1995**, *103*, 8577–8593.
- (43) Banavali, N. K.; Roux, B. Atomic radii for continuum electrostatics calculations on nucleic acids. *J. Phys. Chem. B* **2002**, *106*, 11026–11035.
- (44) McQuarrie, D. A. *Statistical mechanics*; Harper & Row: New York, 1976; pp 136–137.
- (45) Harris, S. A.; Gavathiotis, E.; Searle, M. S.; Orozco, M.; Laughton, C. A. Cooperativity in drug-DNA recognition: a molecular dynamics study. *J. Am. Chem. Soc.* **2001**, *123*, 12658–12663.
- (46) Jusuf, S.; Loll, P.; Axelsen, P. Configurational entropy and cooperativity between ligand binding and dimerization in glycopeptide antibiotics. *J. Am. Chem. Soc.* **2003**, *125* (13), 3988–3994.
- (47) Karplus, M.; Kushick, J. N. Method for estimating the configurational entropy of macromolecules. *Macromolecules* **1981**, *14*, 325–332.
- (48) Levy, R. M.; Karplus, M.; Kushick, J.; Perahia, D. Evaluation of the Configurational entropy for proteins: application to molecular dynamics simulations of an alpha-helix. *Macromolecules* **1984**, *17*, 1370–1375.
- (49) Brooks, B. R.; Janezic, D.; Karplus, M. Harmonic analysis of large systems. I. Methodology. *J. Comput. Chem.* **1995**, *16*, 1522–1542.
- (50) Schlitter, J. Estimation of absolute and relative entropies of macromolecules using the covariance matrix. *Chem. Phys. Lett.* **1993**, *215*, 617–621.
- (51) Andricioaei, I.; Karplus, M. On the calculation of entropy from covariance matrices of the atomic fluctuations. *J. Chem. Phys.* **2001**, *115*, 6289–6292.
- (52) Di Nola, A.; Berendsen, H.; Edholm, O. Free energy determination of polypeptide conformations generated by molecular dynamics. *Macromolecules* **1984**, *17*, 2044–2050.
- (53) Chang, C.; Chen, W.; Gilson, M. Evaluating the accuracy of the quasiharmonic approximation. *J. Chem. Theory Comput.* **2005**, *1*, 1017–1028.
- (54) Sugita, Y.; Okamoto, Y. Replica-exchange molecular dynamics method for protein folding. *Chem. Phys. Lett.* **1999**, *314*, 141–151.
- (55) Hansmann, U. H. E.; Okamoto, Y. New Monte Carlo algorithms for protein folding. *Curr. Opin. Struct. Biol.* **1999**, *9*, 177–183.
- (56) Ryckaert, J.-P.; Ciccotti, G.; Berendsen, H. J. C. Numerical integration of cartesian equations of motion of a system with constraints: molecular dynamics of n-alkanes. *J. Comput. Phys.* **1977**, *23*, 327–341.
- (57) Nose, S. A unified formulation of the constant temperature molecular dynamics methods. *J. Chem. Phys.* **1984**, *81*, 511–519.
- (58) Lee, M. S.; Olson, M. A. Calculation of absolute protein-ligand binding affinity using path and endpoint approaches. *Biophys. J.* **2006**, *90*, 864–877.
- (59) Janezic, D.; Brooks, B. Harmonic analysis of large systems. II. Comparison of different protein models. *J. Comput. Chem.* **1995**, *16*, 1543–1553.

CT6003388